Tracking Biomineralization in Shale Fractures with Magnetic Resonance Velocimetry (MRV) and Micro-CT

Matthew R. Willett[1,2]; Dustin Crandall[3]; Adrienne J. Phillips[2,4]; Sarah L. Codd[2,5], Joseph D. Seymour[1,2]; Catherine M. Kirkland[2,4]

[1]Montana State University, Department of Chemical Engineering, 214 Roberts Hall, Bozeman, MT, USA; [2]Montana State University, Center for Biofilm Engineering, 366 Barnard Hall, Bozeman, MT 59717, USA; [3]National Energy Technology Laboratory, 3610 Collins Ferry Road, Morgantown, WV 26505, USA; [4]Montana State University, Department of Civil Engineering, 205 Cobleigh Hall, Bozeman, MT, USA; [5]Montana State University, Department of Mechanical and Industrial Engineering, 220 Roberts Hall, Bozeman, MT, USA

NATIONAL ENERGY TECHNOLOGY LABORATORY

MONTANA STATE UNIVERSITY

Background

- Shale plays a key role in many geoengineering applications such as hydraulic fracturing and underground energy or carbon storage (Fig. 1).
- Most induced fractures use proppants (e.g., sand) to keep fractures held open over time.
- Methods are needed to control permeability in shale formations to reduce the risk of harmful leakages[1].

Fig. 1: Engineering tools needed for sealing subsurface hydraulic fractures. Figure from [1].

Objectives

- A biofilm-based sealing strategy known as **microbially-induced calcium carbonate precipitation (MICP)** has been demoFnstrated to seal proppant-filled shale rock fractures under subsurface conditions (Fig. 2)[2].
- Fluid-rock interactions that drive mineral precipitation inside the fracture are not well studied.
- We used two non-invasive techniques to study how biomineralization affects fluid flow in shale fractures: **micro-CT** and **magnetic resonance velocimetry (MRV)**

Microbially-Induced Calcium Carbonate Precipitation

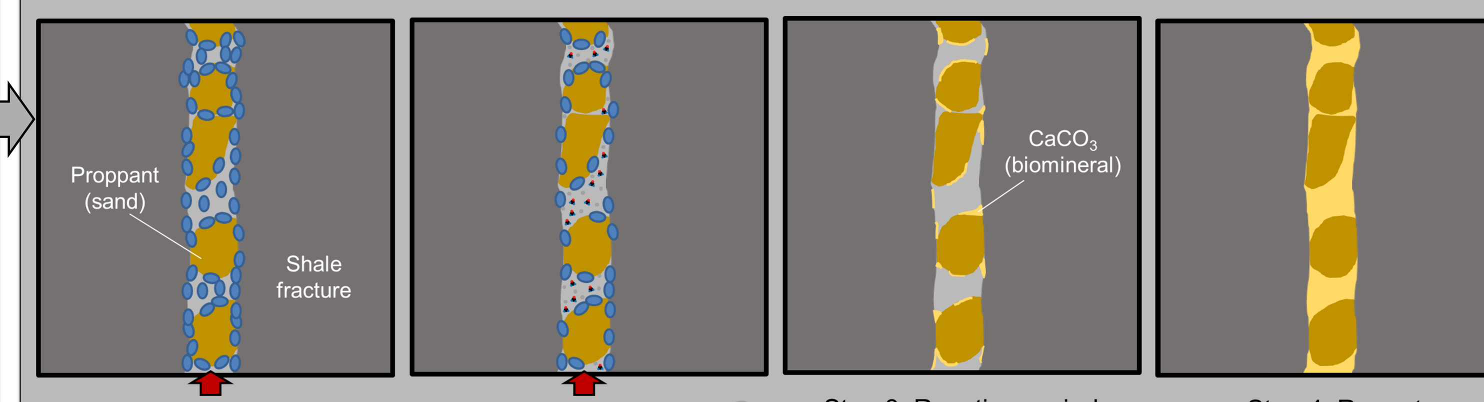

Step 1: Inject microbes (*S. pasteurii*) & attachment period

Step 2: Add reactants (urea and calcium)

Step 3: Reaction period

Step 4: Repeat

Fig. 2. Overview of MICP-treatment for fracture sealing.

$$CO(NH_2)_2 + 2H_2O + Ca^{2+} \xrightarrow{urease} 2NH_4^+ + CaCO_3(s)$$

Micro-CT and Modified Local Cubic Law (MLCL) Flow Simulation

- Micro-CT takes multiple X-ray measurements at different angles around a sample.
- 2D cross-sectional images are reconstructed from the 1D X-Ray projections.
- Micro-CT cannot visualize fracture flow, but this can be simulated through modeling.
- Modified local cubic law (MLCL) model was used to predict 2D flow from CT calculated aperture map (Fig. 3).

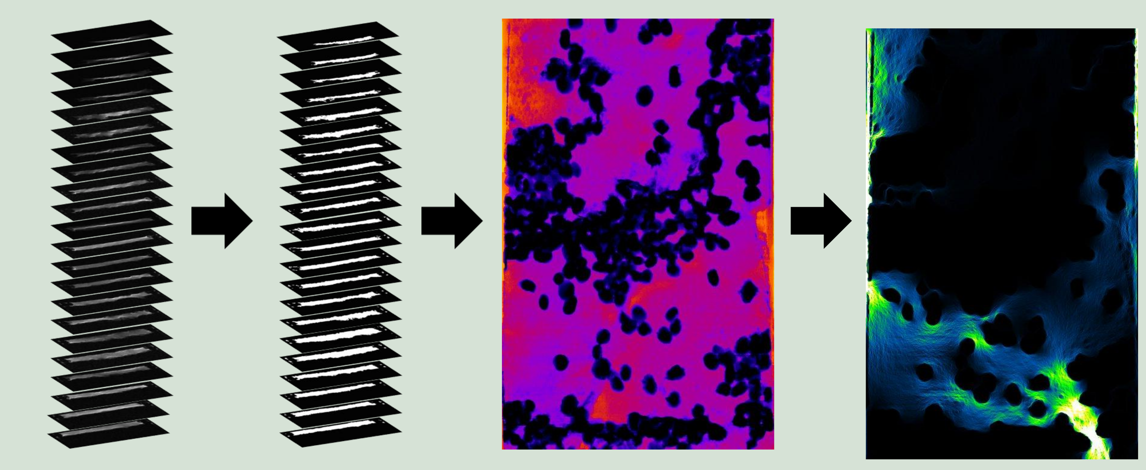

Fig. 3. Workflow of processing micro-CT images for fracture flow simulation.

Magnetic Resonance Velocimetry (MRV)

- **Magnetic resonance imaging** (MRI) uses magnetic field gradients to image [1]H nuclei (also known as "spins") non-invasively (Fig. 4)[3].
- **Pulsed field gradient nuclear magnetic resonance (PFG NMR)** is an experimental technique used to measure flow and diffusion properties. A pair of pulsed field gradients imparts a phase shift ($\Delta\Phi$) on the spins' rotation that depends on the spins' motion (Fig. 4)[3].
- PFG NMR can be used to measure the probability distribution of spin displacements called a **propagator**.
- **Magnetic resonance velocimetry** (MRV) combines MRI and PFG NMR to create spatial velocity maps.

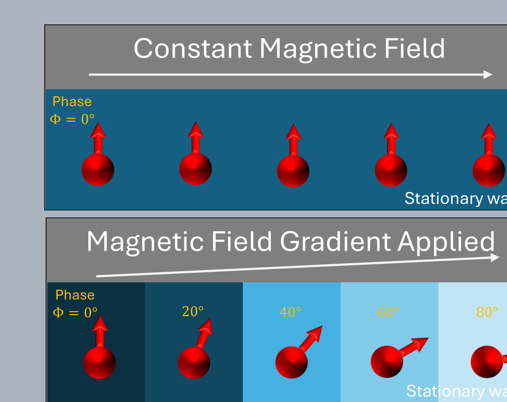

Fig. 4. In the presence of a magnetic field gradient (bottom), spins acquire a phase shift in their rotation. PFG NMR applies a pair of magnetic field gradients that refocuses the phase of stationary spins, but the residual phase of moving spins is measured and used to calculate velocity. Figure modified from [4].

Micro-CT Experimental Setup

- North Star Imaging M-5000 industrial CT scanner (NETL).
- VorteX scan with 3600 projections
- Imaging analysis in FIJI with Labkit segmentation.
- Modified LCL simulation developed by Matt Stadelman[5] based on model of Brush and Thomson[6].

Resolution	✓	22 μm (x) 22 μm (y) 22 μm (z)
Non-invasive	✓	
Measure flow quantities		Not directly; 2D flow simulation

Samples & Sealing Strategy

- 2-inch long, 1-inch diameter Marcellus shale
- Pulsed-flow, staged injection MICP treatment
- 3 flow-through cases studied:

MRV Experimental Setup

- Bruker AVANCE 300 MHz at Magnetic Resonance Lab (MSU).
- 2-step, pulsed gradient spin echo (PGSE) pulse sequence for spatial (average) velocity maps.
- PGSE pulse sequence for (bulk) propagators.

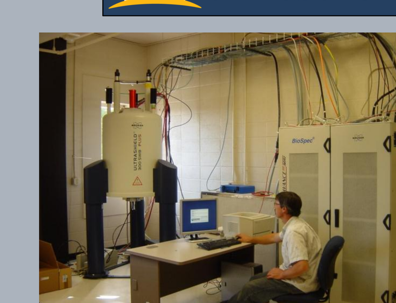

Resolution		234 μm (x) 117 μm (y) 1000 μm (z)
Non-invasive	✓	
Measure flow quantities	✓	(in 3D)

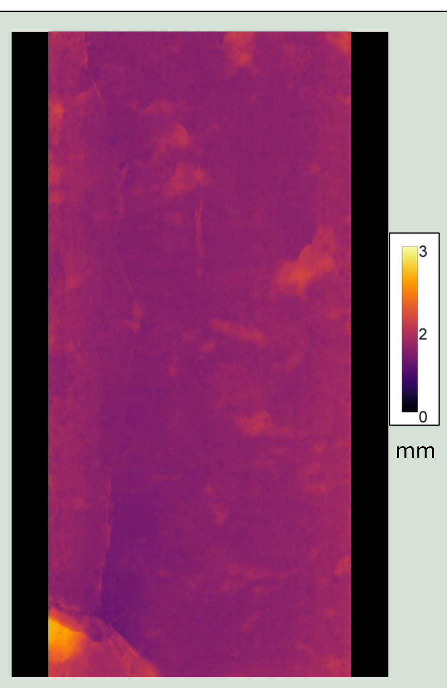

Fig. 5. Fracture aperture map of shale fracture calculated from micro-CT images.

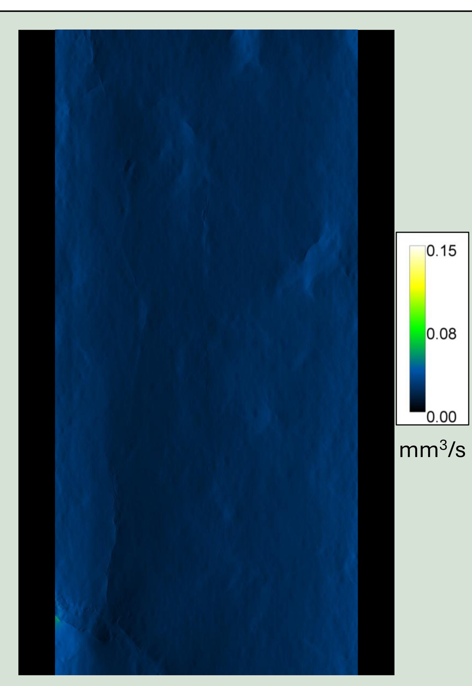

Fig. 6. Fracture flow map of shale fracture from MLCL simulation. Flow is uniform throughout.

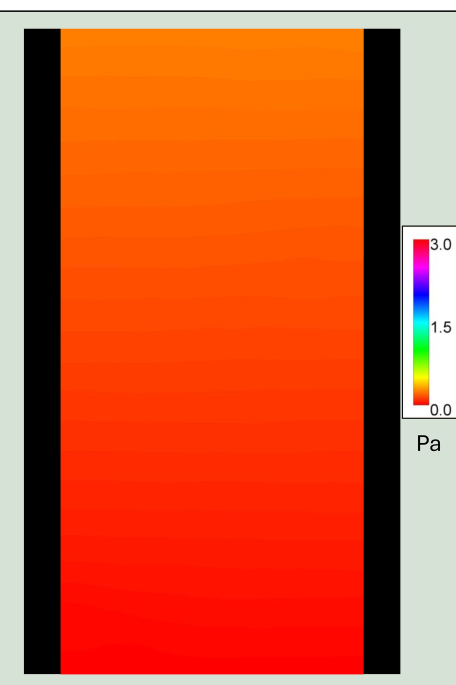

Fig. 7. Pressure distribution map of shale fracture from MLCL simulation.

1

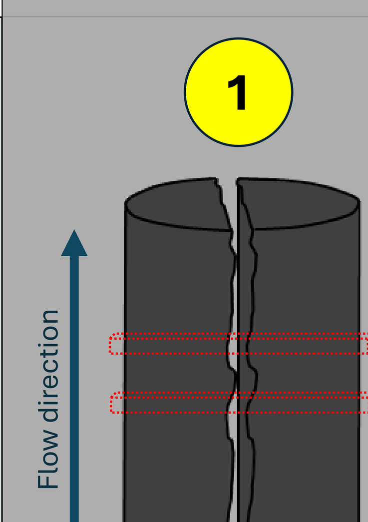

Shale Fracture

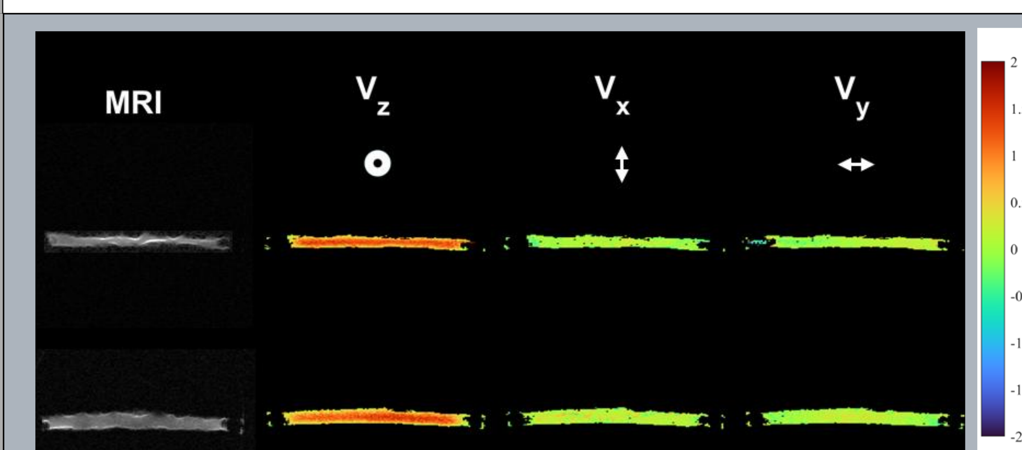

Fig. 8. Cross-sectional MRI/Velocity maps of flow through shale fracture showing 3D encoded velocities (as illustrated in red "slices" in cartoon)

- Flow is concentrated in the main direction of fluid flow (z-direction) (Fig. 8).
- Measured velocities are proportional to the imposed flowrate (Fig. 9)
- 1D profiles of v_z across the aperture are parabolic, though many are offset from the fracture midpoint due to rough surfaces (Figs. 9-10).

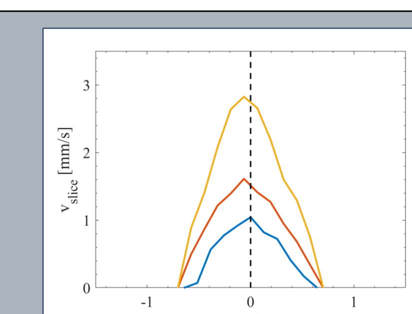

Fig. 9. 1D v_z profile at varying flow rates.

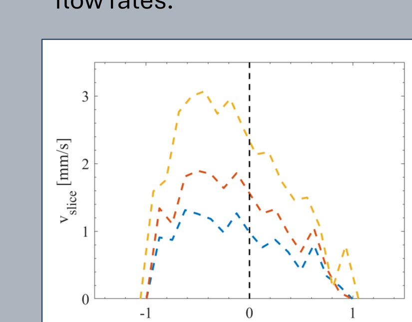

Fig. 10. Alternative 1D v_z profile at varying flow rates.

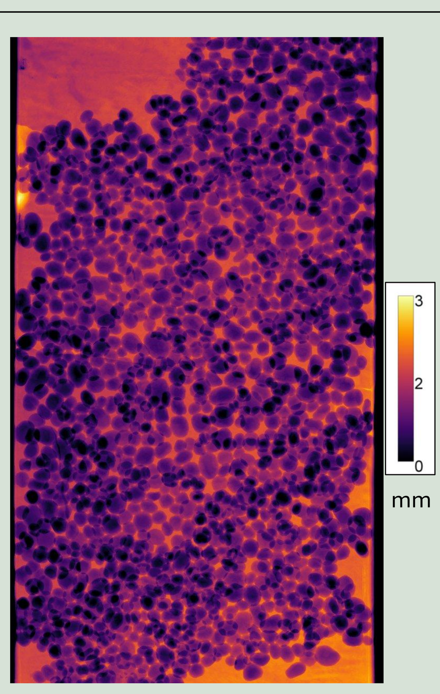

Fig. 11. Fracture aperture map of shale fracture with proppant.

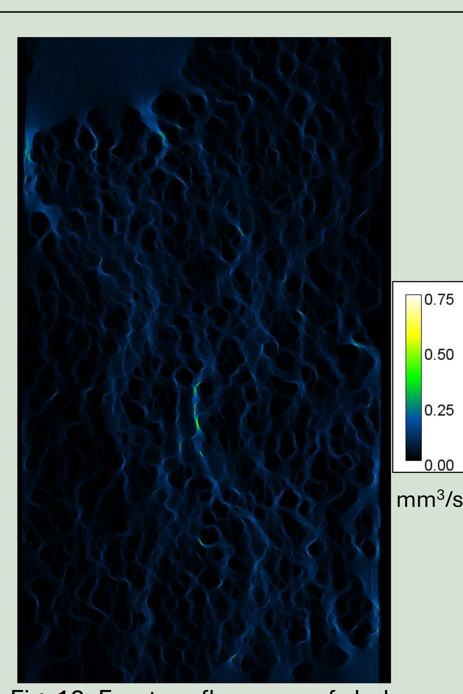

Fig. 12. Fracture flow map of shale fracture with proppant from MLCL simulation. Flow channeling is observable

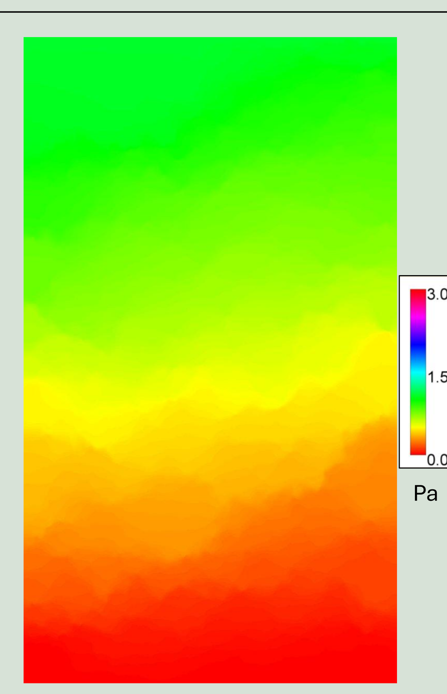

Fig. 13. Pressure distribution map of shale fracture with proppant from MLCL simulation.

2

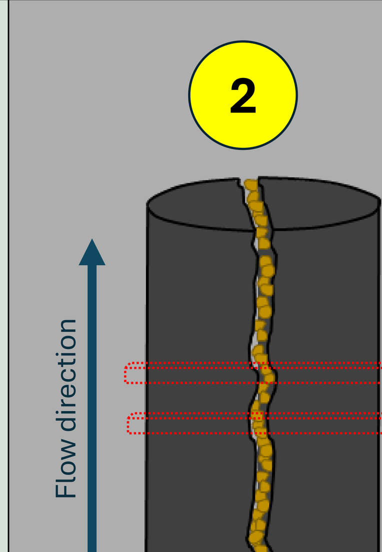

Shale Fracture with Proppant

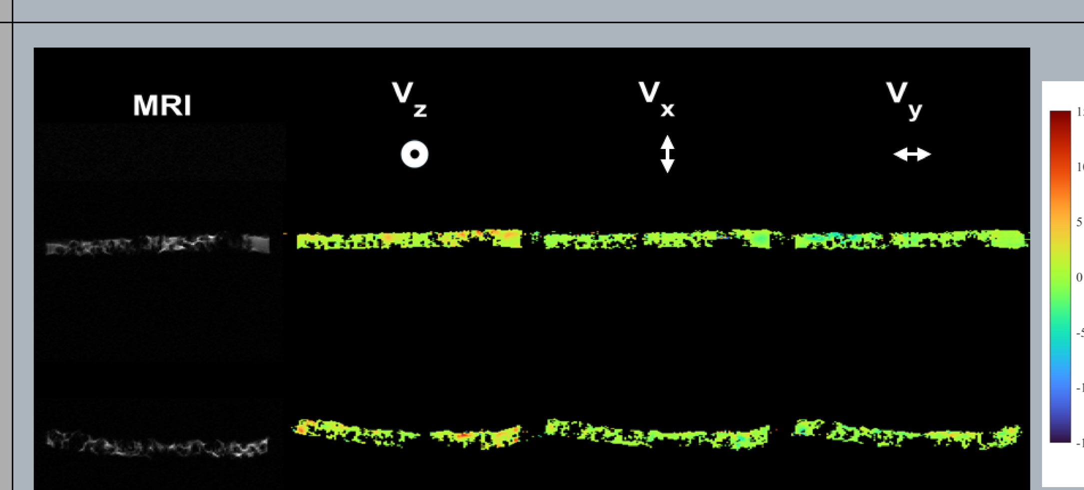

Fig. 14. Cross-sectional MRI/Velocity maps of flow through shale fracture with proppant showing 3D encoded velocities (as illustrated in red "slices" in cartoon).

- Flow channelization observable after the addition of proppant (Fig. 14)
- Bulk propagators confirm that flow moves through more preferential flowpaths at higher flowrates (Fig. 15)
- Good agreement between propagators and spatial velocity maps (Fig. 16)

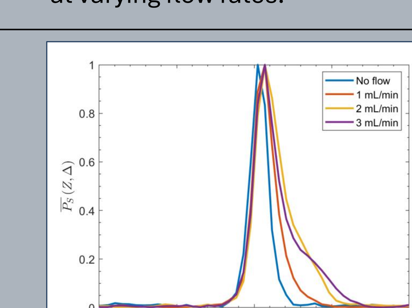

Fig. 15. Bulk propagators at varying flow rates.

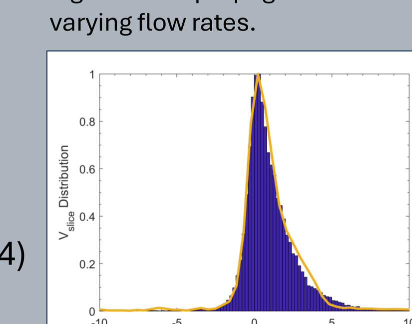

Fig. 16. Comparing propagator (yellow) with histogram of spatially encoded velocities (purple).

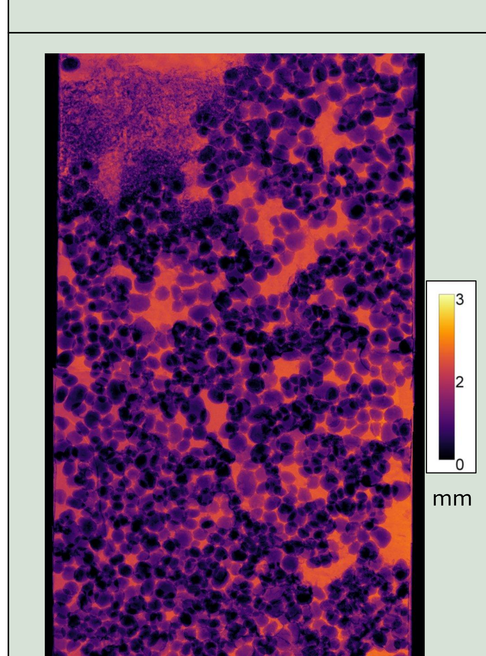

Fig. 17. Fracture aperture map of biomineralized shale fracture with proppant. Mineral buildup and more zones with zero aperture are observable.

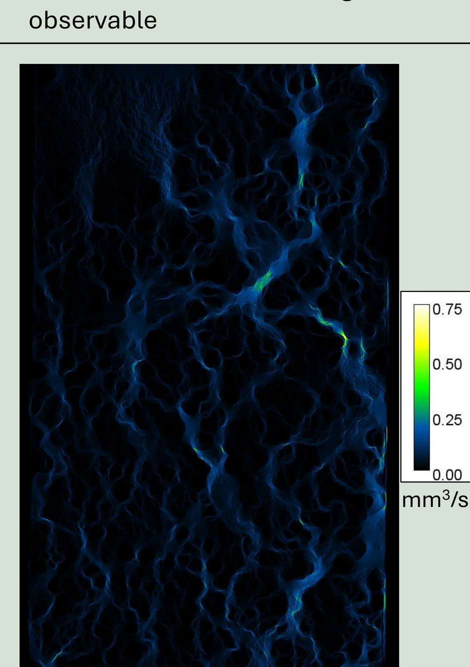

Fig. 18. Fracture flow map of biomineralized shale fracture with proppant from MLCL simulation. There are fewer available flow paths after MICP-treatment.

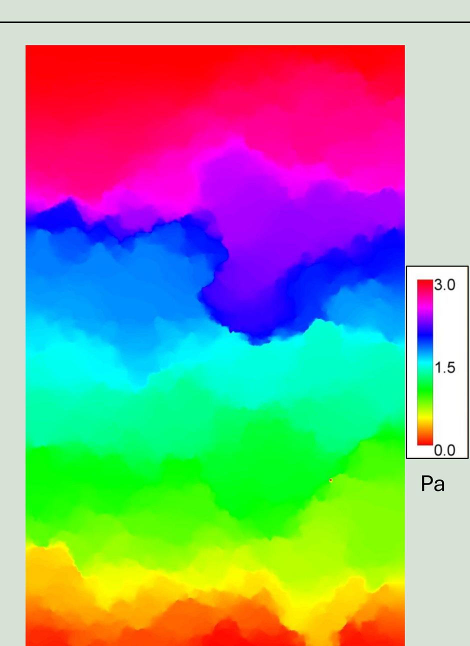

Fig. 19. Pressure distribution map of biomineralized shale fracture with proppant from MLCL simulation.

3

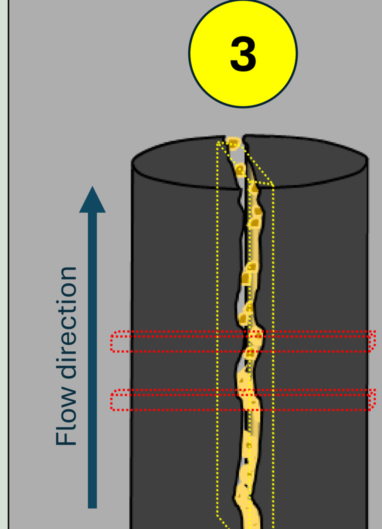

Biomineralized Shale Fracture with Proppant

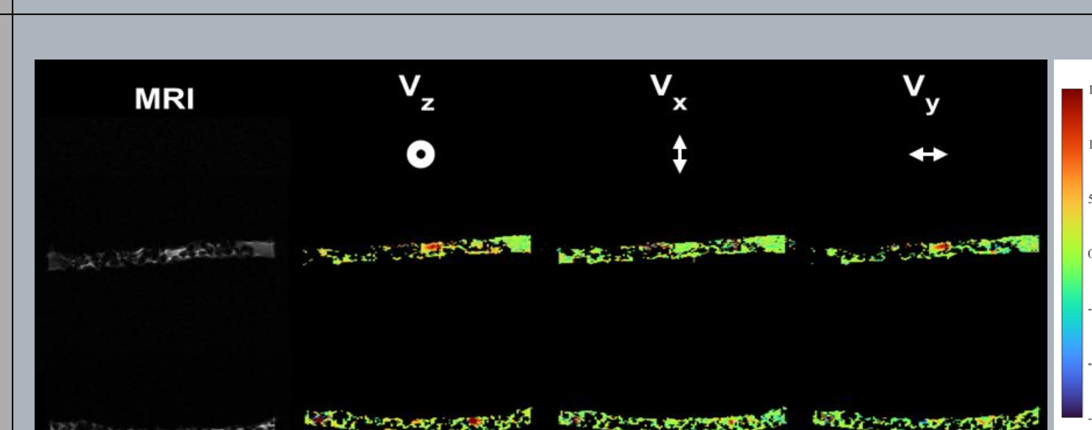

Fig. 20. Cross-sectional MRI/Velocity maps of flow through biomineralized shale fracture with proppant showing 3D encoded velocities (as illustrated in red "slices" in cartoon).

- After biomineralization, flow become even more non-uniform (Fig. 20).
- MRV images can be acquired in any orientation, and longitudinal maps present a way to view the full flow field (Fig. 21)
- Longitudinal maps highlight the main preferential flow path (Fig. 21)

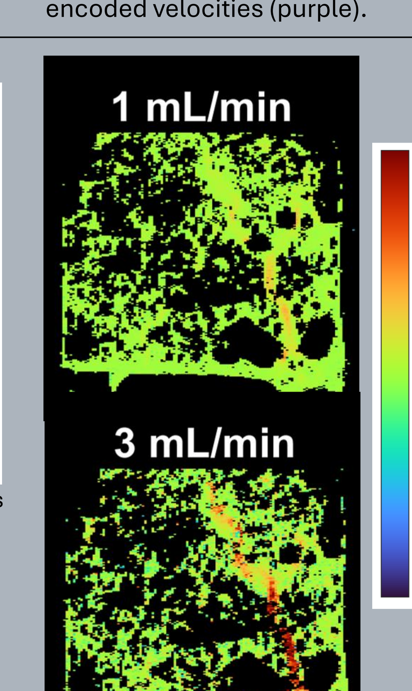

Fig. 21. Longitudinal velocity map at varying flow rates (as illustrated in yellow "slice" in cartoon).

References

1. Phillips, A. J., Gerlach, R., Lauchnor, E., Mitchell, A. C., Cunningham, A. B., & Spangler, L. (2013). Engineered applications of ureolytic biomineralization: a review. Biofouling, 29(6), 715–733.
2. Willett, M.R., Bedey, K., Crandall, D. et al. (2024). Beyond the Surface: Non-Invasive Low-Field NMR Analysis of Microbially-Induced Calcium Carbonate Precipitation in Shale Fractures. Rock Mech Rock Eng.
3. Callaghan, Paul T (2011). Translational Dynamics and Magnetic Resonance: Principles of Pulsed Gradient Spin Echo NMR. Oxford.
4. Lotz, J., Meier, C., Leppert, A., & Galanski, M. (2002). Cardiovascular flow measurement with phase-contrast MR imaging: basic facts and implementation. Radiographics, 22(3), 651–671.
5. Stadelman, M. A. (2017). Comparing the Hydrodynamic Response of Fracture Shearing in Marcellus and Eau Claire Shales. West Virginia University.
6. Brush, D. J., and N. R. Thomson (2003). Fluid flow in synthetic rough-walled fractures: Navier-Stokes, Stokes, and local cubic law simulations, Water Resour. Res., 39, 1085.

U.S. DEPARTMENT of ENERGY